PAPER

Anomalous charge density wave state evolution and dome-like superconductivity in $CuIr_2Te_{4-x}Se_x$ chalcogenides

To cite this article: Mebrouka Boubeche *et al* 2021 *Supercond. Sci. Technol.* **34** 115003

View the article online for updates and enhancements.

Anomalous charge density wave state evolution and dome-like superconductivity in CuIr$_2$Te$_{4-x}$Se$_x$ chalcogenides

Mebrouka Boubeche[1], **Ningning Wang**[2], **Jianping Sun**[2], **Pengtao Yang**[2], **Lingyong Zeng**[1], **Qizhi Li**[3], **Yiyi He**[1], **Shaojuan Luo**[4], **Jinguang Cheng**[2] (iD), **Yingying Peng**[3] (iD) **and Huixia Luo**[1,*] (iD)

[1] School of Materials Science and Engineering, State Key Laboratory of Optoelectronic Materials and Technologies, Key Laboratory of Polymer Composite and Functional Materials, Sun Yat-Sen University, No. 135, Xingang Xi Road, Guangzhou 510275, People's Republic of China
[2] Beijing National Laboratory for Condensed Matter Physics and Institute of Physics, Chinese Academy of Sciences and School of Physical Sciences, University of Chinese Academy of Sciences, Beijing 100190, People's Republic of China
[3] International Center for Quantum Materials, School of Physics, Peking University, Beijing 100871, People's Republic of China
[4] School of Chemical Engineering and Light Industry, Guangdong University of Technology, Guangzhou 510006, People's Republic of China

E-mail: luohx7@mail.sysu.edu.cn

Abstract

We report the anomalous charge density wave (CDW) state evolution and dome-like superconductivity in CuIr$_2$Te$_{4-x}$Se$_x$ ($0 \leqslant x \leqslant 0.5$) series. Room temperature powder x-ray diffraction (XRD) results indicate that CuIr$_2$Te$_{4-x}$Se$_x$ ($0 \leqslant x \leqslant 0.5$) compounds retain the same structure as the host CuIr$_2$Te$_4$ and the unit cell constants a and c manifest a linear decline with increasing Se content. Magnetization, resistivity and heat capacity results suggest that superconducting transition temperature (T_c) exhibits a weak dome-like variation as substituting Te by Se with the maximum $T_c = 2.83$ K for $x = 0.1$ followed by suppression in T_c and simultaneous decrease of the superconducting volume fraction. Unexpectedly, the CDW-like transition (T_{CDW}) is suppressed with lower Se doping ($0.025 \leqslant x \leqslant 0.2$) but re-emerges at higher doping ($0.25 \leqslant x \leqslant 0.5$). Meanwhile, the temperature-dependent XRD measurements show that the trigonal structure is stable at 20 K, 100 K and 300 K for the host sample and the doping composition with $x = 0.5$, thus we propose that the behavior CDW-like transition arises from the disorder effect created by chemical doping and is not related to structural transition. The lower and the upper critical fields of these compounds are also addressed.

* Author to whom any correspondence should be addressed.

1. Introduction

Transition-metal chalcogenides (TMCs) own plentiful structural chemistry and physical properties such as nontrivial topological properties [1–3], charge density wave (CDW) [4–6], superconductivity (SC) [7–10], Mott transition [11], extremely large magnetoresistance [12, 13], spin glass [14], and so on. Specifically, the coexistence/competition of SC and CDW is a long history but still a hot topic in condensed matter physics. CDW and SC are two fully distinct cooperative states, both of which happen because of the instabilities of Fermi surface (FS) that result in the splitting of FS and the density of states (DOS) at FS surface decrease below their corresponding transition temperatures. So far, abundant results demonstrate that a superconducting dome can usually be seen on the edge of a CDW/structural instability by the application of hydrostatic pressure [15, 16], chemical doping [17–22], or gating [23]. Among chemical doping methods, the isovalent substitution is a commonly used strategy to study the key relation between SC and instabilities in some other order parameters. A recent, prominent case is $1T\text{-}TaS_{2-x}Se_x$, in which SC occurs when the commensurate CDW (CCDW) Mott phase vanishes, and it coexists with the nearly CCDW state [24]. Moreover, the isoelectronic S substitution for Se in $2H\text{-}TaSe_2$ leads to the emergence of a robust superconducting order in the $2H\text{-}TaSe_{2-x}S_x$ ($0 \leqslant x \leqslant 2$) series. In the case of $2H\text{-}TaSe_{2-x}S_x$ ($0 \leqslant x \leqslant 2$) compounds, the CDW is suppressed and the SC is maximized with crystallographic disorder, and the superconducting transition temperature (T_c) of the doped compound is surprisingly higher than those of two end compounds [25]. Another example of isoelectronic substitution material is $TaSe_{2-x}Te_x$ ($0 \leqslant x \leqslant 2$). The isoelectronic Te replacement for Se in $2H\text{-}TaSe_2$ not only leads to two polytypes and two polymorphs, but also enhances the T_c. The T_cs of the 1T and 3R polymorph $TaSe_{2-x}Te_x$ are both higher than that of the undoped $2H\text{-}TaSe_2$. Especially, the maximum T_c of $3R\text{-}TaSe_{2-x}Te_x$ variants is five times larger than that of the undoped $2H\text{-}TaSe_2$ sample [26]. Moreover, the $3R\text{-}TaSe_{2-x}Te_x$ variants exhibit the coexistence of SC and CDW, with $3R\text{-}TaSe_{1.9}Te_{0.1}$ initially displaying an incommensurate and then transitioning to a CCDW phase upon further cooling. This phenomenon likely emerges either from an unexpected influence of the layer stacking order on the electronic properties, which is likely to be dominated by the characteristics of the single layer or from exceptional dependence of T_c on the subtle differences in the properties of the single layers in this type of compounds [26]. Besides, SC is emerged or enhanced upon isoelectronic Se substitution for Te/S in the parent TMCs (e.g. $1T\text{-}PdTe_2$, $1T\text{-}TaS_2$, $ZrTe_3$) [27–30]. The enhancement of T_c in $1T\text{-}PdSeTe$ is considered to be arising from the possible existence of metallic Pd or PdTe stripes and/or some dedicated structural disorder caused by a rather small amount of Se deficiency. Except for the TMC compounds, Se chemical doping has been confirmed to be an effective tool to tune the CDW and SC in other systems like $Eu_3Bi_2S_4F_4$ [31], $Nb_2Pd(S_{1-x}Se_x)_5$ [32] and so on.

Very recently, the occurrence of SC in a CDW materials has been observed in the quasi-two-dimensional $Cu_{0.5}IrTe_2$ ($CuIr_2Te_4$) chalcogenides with a NiAs defected trigonal structure (space group $P3\text{-}m1$) as presented in the inset of figure 1(a), in which Cu is intercalated between the Te–Ir–Te layers [33]. The T_c is around 2.5 K, and the CDW transition temperature (T_{CDW}) is about 250 K (from heating) and 186 K (from cooling). First-principles calculations further reveal that the electronic DOS in the vicinity of the Fermi energy fundamentally descend from the Ir d and Te p orbitals [33]. Therefore, it is reasonable to tune the SC and CDW in the parent $CuIr_2Te_4$ telluride chalcogenide with isoelectronic Se substitution for Te-site by controlling the Fermi energy E_F or creating disorder.

On the other hand, copper-based chalcogenide spinels display rich physical properties such as magnetic ordering [34–36], metal-insulator transition (MIT) [37–39], and SC [8, 40–42]. It is well known that the sulpo-$CuRh_2S_4$, where the Cu atoms occupy the tetrahedra sites and the Rh atoms occupy the octahedra sites, shows SC with $T_c = 4.70$ K [31]. Another spinel $CuIr_2S_4$ displays temperature-induced MIT near 226 K with structural phase transition, displaying hysteresis on cooling and heating [39]. Selenospinel $CuIr_2Se_4$ (isostructural to $CuIr_2S_4$), however, remains ordinary metal above 0.5 K at ambient pressure but shows a MIT above 2.8 GPa [43, 44]. Despite the absence of metal–metal pairing or charge ordering in $CuIr_2Se_4$, it seems to be at the margin of such performance [45], i.e. it possibly has a nascent propensity to such fluctuation due to the robust spin–orbit coupling of 5*d* Ir and the geometrical frustration inherent to the spinel structure. Indeed, SC in $CuIr_2Se_4$ spinel has been prompted by Pt substitution for Ir [8]. Therefore, these differences in structural and electronic properties between the layered $CuIr_2Te_4$ and the spinel $CuIr_2Se_4$ have attracted our attention as a starting point to explore the effect of the isoelectronic Se substitution for Te site on the SC and CDW in $CuIr_2Te_4$ compound and whether it can facilitate SC near a CDW state.

For this matter, we successfully synthesized and systemically investigated the crystallographic and physical properties of the polycrystalline $CuIr_2Te_{4-x}Se_x$ ($0 \leqslant x \leqslant 0.5$) series. Yet, several attempts have been failed to produce single crystal for this family. The analysis of x-ray diffraction (XRD) measurements under several temperatures (20 K, 100 K and 300 K) indicates that $CuIr_2Te_{4-x}Se_x$ ($0 \leqslant x \leqslant 0.5$) samples maintain the same layered structure as the $CuIr_2Te_4$, but mixed layered phase and cubic phase can be found for $x \geqslant 0.50$ even near
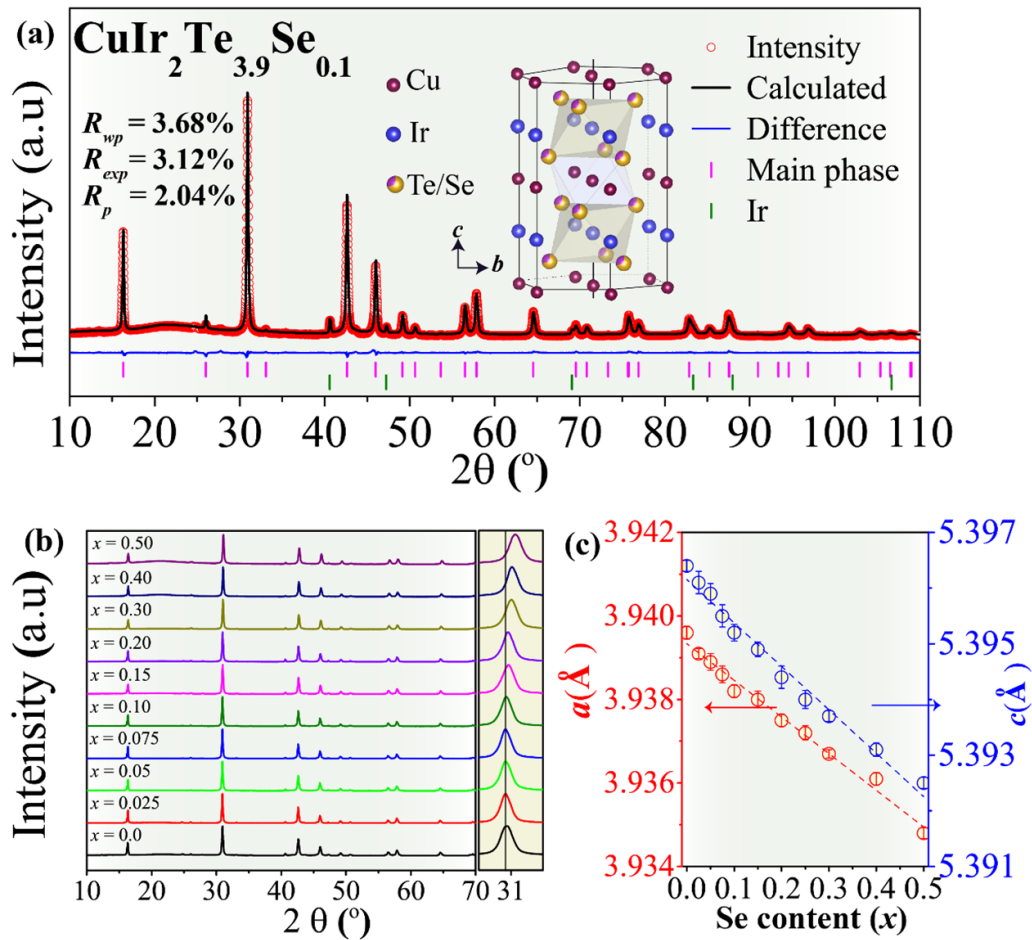
Figure 1. (a) Rietveld refinement for the representative $CuIr_2Te_{3.9}Se_{0.1}$. (b) PXRD patterns for $CuIr_2Te_{4-x}Se_x$ ($0 \leqslant x \leqslant 0.5$). (c) The dependence of unit-cell constants a and c on the doping concentration x.

the end. Resistivity and magnetic susceptibility measurements both show consistently that isoelectronic Se substitution for Te in $CuIr_2Te_4$ first favors the SC near a CDW accompanied with the anomalous CDW state evolution in two sides of dome-like SC. The optimal doping composition is $CuIr_2Te_{0.9}Se_{0.1}$ with the highest $T_c = 2.83$ K. The CDW-like states disappear at lower doping content but re-emerge at higher Se doping concentration.

2. Methods

Polycrystalline $CuIr_2Te_{4-x}Se_x$ ($0 \leqslant x \leqslant 0.5$) compounds are made by means of a vacuum shield solid-state reaction method. Cu, Ir, Te and Se powders were weighted in the stoichiometric ratios and ground with a mortar. Then the mixture was sealed in the evacuated quartz tubes and sintered at 1023 K for 5 d. The as-prepared precursors were then reground, compressed into pellets and heated at 1023 K for 10 d. The polycrystalline $CuIr_2Te_{4-x}Se_x$ samples are not air-sensitive.

To determine phase purity and analyze the detailed crystal structure, powder XRD (PXRD) characterization was carried out at room temperature by using MiniFlex, Rigaku apparatus with Cu Kα1 radiation. Rietveld model in FULLPROF

suite software was used to perform the structural parameter refinements for the obtained polycrystalline $CuIr_2Te_{4-x}Se_x$ compounds. Besides, XRD measurements under 20 K, 100 K and 300 K were carried using a Mo K (17.4 keV) microspot x-ray source and a Pilatus 2D detector. All temperature evolution measurements are conducted through warming process. The elements ratios and their distributions were examined via scanning electronic microscope combined with energy dispersive X-ray spectroscopy (SEM-EDS) EM-30AX PLUS from Kurashiki Kako Co. Ltd, Japan, equipped by an energy dispersive x-ray spectroscopy detector. The temperature-dependent electrical resistivity ($\rho(T)$) of all the samples and the specific heat capacity ($C_p(T)$) measurements we carried out using a quantum design physical property measurement system. The DC magnetic susceptibilities were measured using a superconducting quantum interference device magnetic property measurement system under 10 Oe. Using resistivity $\rho(T)$ data, T_cs are extracted from the midpoint of the drop region, and the extrapolations of the abrupt slope of the susceptibility and the normal state susceptibility, T_c from the specific heat capacity ($C_p(T)$) is estimated by the equal area entropy construction method. T_{CDW} values have been estimated from the minimum of the temperature-dependent derivative of resistivity ($d\rho/dT(T)$) and the maximum of the temperature-dependent

derivative of magnetic susceptibility ($d\chi/dT$) measured under 10 kOe.

3. Results and discussions

We performed detailed structural investigation using the Rietveld refinement technique to check the phase purity and crystal structure of all the synthesized polycrystalline $CuIr_2Te_{4-x}Se_x$ ($0 \leqslant x \leqslant 0.5$) series. The refinement for the representative $CuIr_2Te_{3.9}Se_{0.1}$ compound is shown in figure 1(a). An analysis of XRD patterns shows that $CuIr_2Te_{3.9}Se_{0.1}$ compound has a trigonal structure with lattice contents $a = b = 3.9382$ Å, $c = 5.3952$ Å, which is slightly lower than those of the parent compound $CuIr_2Te_4$ with $a = b = 3.9397$ Å, $c = 5.3964$ Å [32]. The Rietveld refinements for the other investigated polycrystalline samples are depicted in the supplemental information (figure S1 (available online at stacks.iop.org/SUST/34/115003/mmedia)). Besides, the refinement results confirm that all these $CuIr_2Te_{4-x}Se_x$ ($0 \leqslant x \leqslant 0.5$) series preserve the basic trigonal structure with the space group P-$3m1$ as presented in the inset of figure 1(a), though tiny unreacted Ir appears in all the specimens, where Cu atoms occupy the octahedral sites $1b$ (0 0 $1/2$), Ir atoms occupy the sites $1a$ (0 0 0), Te/Se atoms are in sites $2d$ ($1/3$ $2/3$ z). Room temperature XRD patterns of the polycrystalline $CuIr_2Te_{4-x}Se_x$ ($0 < x < 0.5$) compounds are shown in figure 1(b). The variation of the (002) diffraction peaks for different Se concentrations is revealed in the right side of figure 1(b), where all the (002) peaks shift towards higher angle with increasing selenium concentration in $CuIr_2Te_{4-x}Se_x$ ($0 \leqslant x \leqslant 0.5$). Indeed, as depicted in figure 1(c), the lattice constants a and c both manifest linear decrease with the increase of Se concentration x for our synthesized $CuIr_2Te_{4-x}Se_x$, which is in good agreement with Vegard's law [46]. The reason behind this is the smaller ionic radii of Se (1.98 Å) compared with that of Te (2.21 Å) [47]. Hence, a consistent reduction of the unit cell volumes of the $CuIr_2Te_{4-x}Se_x$ compounds is expected. Nevertheless, samples with higher Se content (the vicinity of the spinel $CuIr_2Se_4$) have not been successfully synthesized at present. In addition, we further used scanning electronic microscope combined with energy dispersive X-ray spectroscopy (SEM-EDS) to examine the ratio and the distribution of the elements and found that the experimental percentages of Cu:Ir:Te:Se for $CuIr_2Te_{4-x}Se_x$ samples are close to the initial percentages (see figure S2). As shown in figure S3, we can see a homogeneous distribution for all the elements in these $CuIr_2Te_{4-x}Se_x$ polycrystalline samples.

The raw resistivity data as a function of temperature is plotted in figure S4. The temperature-dependent normalized resistivity (ρ/ρ_{300K}) of $CuIr_2Te_{4-x}Se_x$ ($0 \leqslant x \leqslant 0.5$) polycrystalline series under zero magnetic field is given in figure 2(a). The specimens demonstrate a metallic behaviour in the temperature region of 3 K – 300 K, but there is abnormal hump in some samples. A sharp drop of resistivity can be seen at low temperatures, identifying the onset of SC. Normalized resistivity ρ/ρ_{300K} near T_c is shown in

figure 2(b). T_c gradually increases up to 2.83 K for the optimal $CuIr_2Te_{3.9}Se_{0.1}$. From table 1 and figure S5, we can see that the increase of T_c is followed in an increase residual resistivity ratio (RRR $= R_{300K}/R_{8K}$) from 4.16 for the undoped sample to 5.88 for the doped sample with the highest T_c ($x = 0.1$). Besides, from figure 2(a), we can see that the anomalies hump disappears at very low Se doping concentration region, indicating the suppression of CDW-like transition temperatures (T_{CDW}), which is determined by the minimum of $d\rho/dT$ (see inset of figure 2(a)). Meanwhile, the Se doped samples in the region of $0 < x \leqslant 0.3$ exhibit sharp superconducting transition, implying that the samples is highly homogeneous (see figure 2(b) and table 1). Unexpectedly, the hump anomalies associated with CDW-like transition in the $\rho(T)$ curves re-emerges when $x = 0.25$. For $0.25 \leqslant x \leqslant 0.5$, the T_{CDW} transition anomalies steadily increases with increasing Se doping, while the RRR (RRR $= R_{300K}/R_{8K}$) sharply decreases from 3.02 for $x = 0.25$–1.87 for $x = 0.5$ (see table 1 and figure S5). The decrease of RRR suggests that Se doping induces disorder significantly and Se ions are effective scattering centers [48–50], which could account for the reemergence of the CDW.

The magnetic susceptibility measurement provides substantial evidence for bulk SC. The zero-field cooling temperature dependence of the normalized magnetization ($4\pi\chi$) data under 10 Oe for $CuIr_2Te_{4-x}Se_x$ samples are given in figures 2(c) and S5, which display a diamagnetic behavior below T_cs. The change in T_cS is found to be in good agreement with the electrical transport data, whereas the superconducting volume fraction is getting smaller with higher doping content. In particular, the superconducting volume fraction for those samples with the re-emergence of CDW-like transition for $x \geqslant 0.25$ is much smaller than those of other samples without CDW-like transition, suggesting the competition between SC and CDW-like transition. We further performed the magnetization hysteresis under 10 kOe from cooling and heating process as shown in figures 2(d) and S5, these compounds with $x \geqslant 0.25$ also exhibit the CDW-like related magnetic anomalies. The inset in figure 2(d) represents the cooling temperature differentiated magnetization ($d\chi/dT(T)$) curves that have been used to define the values of T_{CDW}. These values are in good agreement with those data derived from $\rho(T)$ measurements.

With the purpose of revealing whether the abnormal hump is related to a structural phase transition, we have performed XRD measurements on the parent $CuIr_2Te_4$ and highest doping sample $CuIr_2Te_{3.5}Se_{0.5}$ at 20 K, 100 K and 300 K. From figure 3, we can see that the three XRD patterns measured at different temperature are similar, which can be successfully indexed to the space group $P3$-$m1$. Thus, the abnormal hump is likely not linked to the structural transition. It indicates that there is no structural phase transition at low temperature, which differs from the case for $IrTe_2$ where the resistivity anomaly has been proved associated to the structural phase transition from trigonal to monoclinic structure at cooling [18, 20, 51]. However, there is no strong CDW signal can be detected, which may be ascribed to the polycrystalline nature of our samples. We have also realized
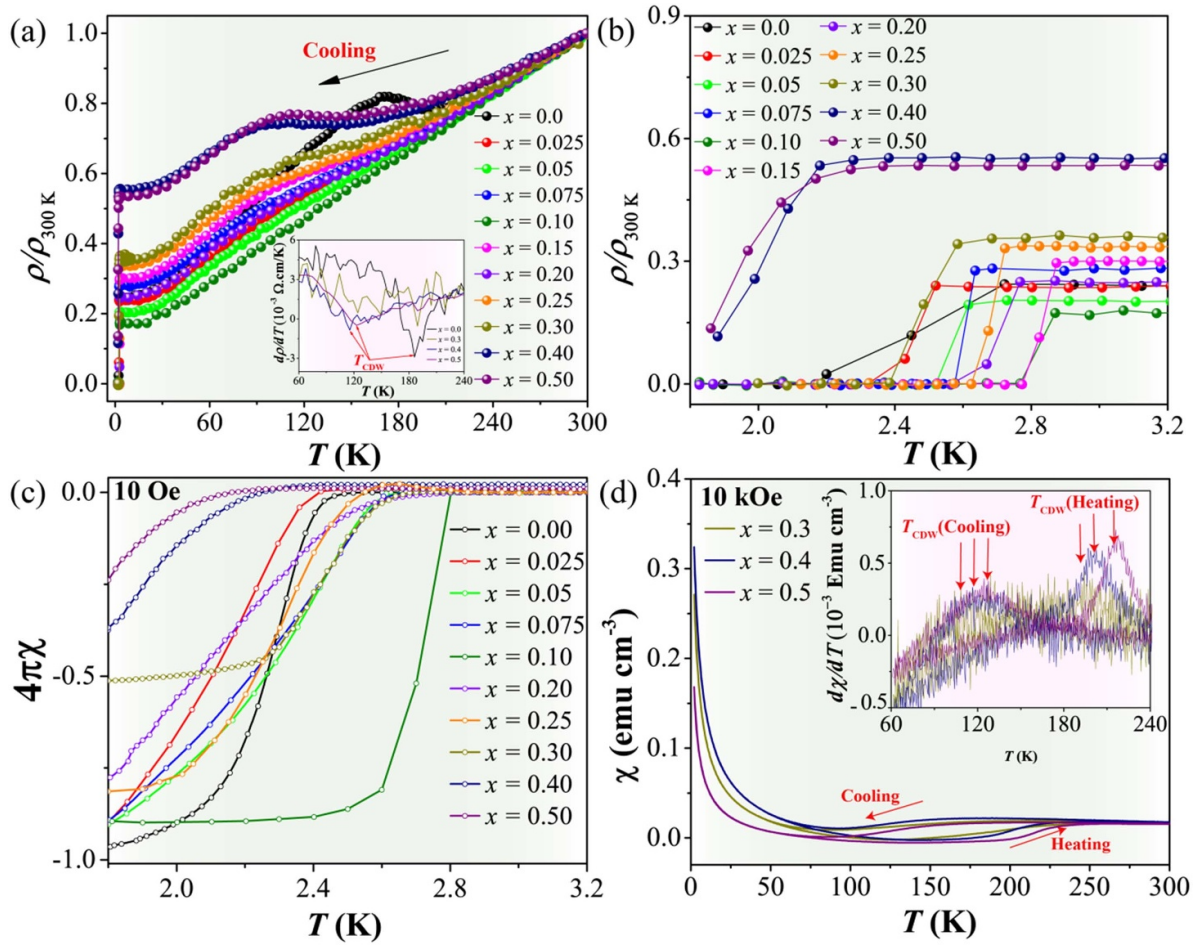
Figure 2. Electrical transport and magnetic properties of $CuIr_2Te_{4-x}Se_x$. (a) The temperature-dependent resistivity for the polycrystalline $CuIr_2Te_{4-x}Se_x$. (b) The magnified view of the normalized resistivity (ρ/ρ_{300K}) at the superconducting transition range for the polycrystalline $CuIr_2Te_{4-x}Se_x$ at low temperatures. (c) Magnetic susceptibilities for $CuIr_2Te_{4-x}Se_x$ ($0 \leqslant x \leqslant 0.5$) near the superconducting transitions region measured under 10 Oe applied field. (d) Magnetization curves measured under 10 kOe for $CuIr_2Te_{4-x}Se_x$ ($0.3 \leqslant x \leqslant 0.5$).

Table 1. Se content (x) dependence of the residual resistance ratio (RRR $= R_{300K}/R_{8K}$), superconducting transition temperature (T_c), and CDW transition temperature (T_{CDW}).

Se content (x)	RRR $= R_{300K}/R_{8K}$	T_c (K)	T_{CDW} (K)
0	4.16	2.50	187
0.025	4.34	2.48	—
0.05	4.87	2.58	—
0.075	3.70	2.61	—
0.1	5.88	2.83	—
0.15	3.49	2.82	—
0.2	4.16	2.71	—
0.25	3.02	2.68	100
0.3	2.71	2.50	108
0.4	1.81	2.05	116
0.5	1.87	1.94	131

that it will be more clearly if the observed abnormal humps appear in the crystalline samples instead of the polycrystalline compounds. However, we have tried a few methods including self-flux method, vapor transport method and modified Bridgman method to grow the crystalline samples, but all failed to obtain the target crystalline samples so far.

To further confirm the bulk SC in the $CuIr_2Te_{4-x}Se_x$ system, the optimal doping polycrystalline $CuIr_2Te_{3.9}Se_{0.1}$ composition is characterized by low-temperature specific heat capacity (C_p) measurement. The main panel of figure 4(a) displays the plots of C_p/T against T^2 for 0 and 10 kOe applied fields. A clear sharp anomaly in zero magnetic field is observed around 2.81 K as presented in the inset figure 4(a), which is close to that determined by the resistivity and susceptibility. Besides, the specific heat jump is suppressed upon the application of the magnetic field 10 kOe, indicating that the upper critical field for $CuIr_2Te_{3.9}Se_{0.1}$ is less than 10 kOe. The zero-field specific heat above T_c can be well fitted to $C_p/T = \gamma + \beta T^2$ (see the dashed red line in figure 4(a)), where γ is the constant of electronic contribution to the specific heat ($C_{el.}$) and β is the lattice constants in the second term of the phonon contribution ($C_{ph.}$). γ value is about 10.84 mJ mol^{-1} K^{-2}, and β value is near 3.51 mJ mol^{-1} K^{-4}. Further, the Debye temperature (Θ_D) can be calculated from the formula $\Theta_D = (12\pi^4 nR/5\beta)^{1/3}$, where $n = 7$ is the number of atoms per formula unit and R is the gas constant. Θ_D value for the
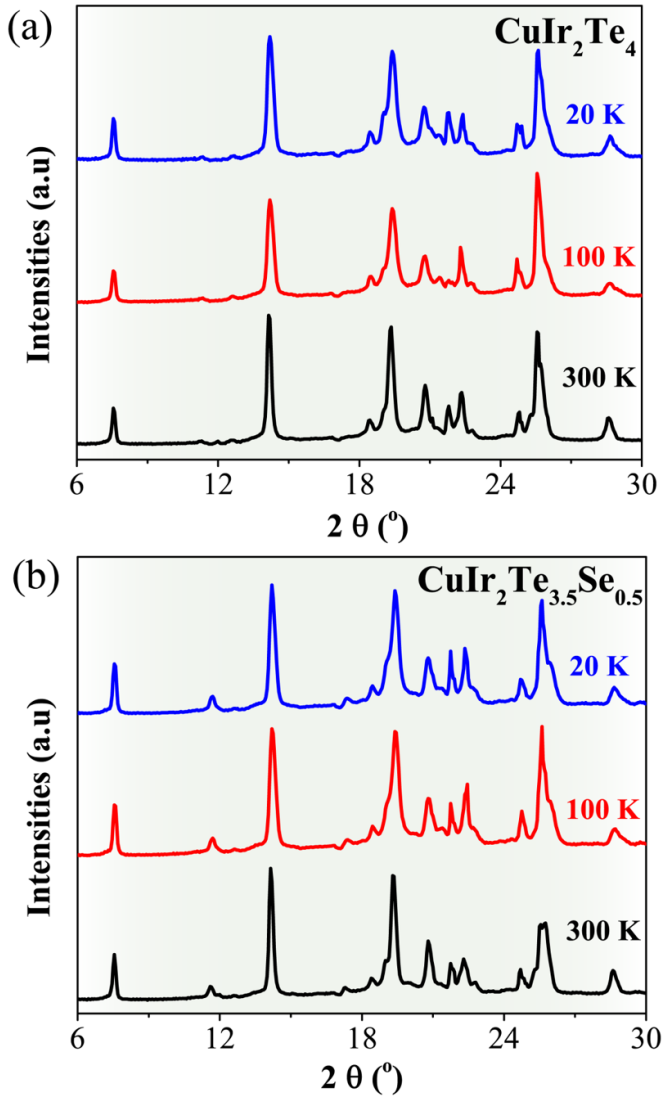
Figure 3. Temperature-dependent PXRD patterns for the representative samples: (a) $CuIr_2Te_4$ and (b) $CuIr_2Te_{3.5}Se_{0.5}$ at 20 K, 100 K and 300 K.

$CuIr_2Te_{3.9}Se_{0.1}$ sample is 157 K. Hereafter, we calculated the electron–phonon coupling constant (λ_{ep}) using the value of Θ_D and T_c values from the inverted McMillan equation [52]: $\lambda_{ep} = \frac{1.04 + \mu * \ln(\Theta_D / 1.45 T_c)}{(1 - 0.62 \mu *) \ln(\Theta_D / 1.45 T_c) - 1.04}$, where $\mu^* = 0.15$ is the repulsive screened coulomb parameter. The value of λ_{ep} is estimated to be 0.65. We then calculated the DOS at the Fermi level $N(E_F)$ from the formula $N(E_F) = 3\gamma / (\pi^2 k_B^2 (1 + \lambda_{ep}))$, where k_B is Boltzmann's constant. $N(E_F)$ is calculated to be 3.11 states/eV/f.u. (f.u. = formula unit), which is little higher then that of the pristine $CuIr_2Te_4$. The enhancement in the SC in $CuIr_2Te_{4-x}Se_x$ compounds can be explained according to the enhancement of the electron–phonon coupling (λ_{ep}) and the increase of DOS of FS $N(E_F)$ by Se substitution as compared to the host $CuIr_2Te_4$. We calculated the specific heat jump ΔC ($T = T_c$) as the difference between the $C_{el.}$ at T_c and the normal state (illustrated by the solid red line in the inset of figure 4(a). The normalized specific heat jump value $\Delta C_{el.} / \gamma T_c$ is estimated to be 1.51, which is slightly higher

the Bardeen–Cooper–Schrieffer (BCS) weak-coupling limit (1.43), which confirm the bulk nature of SC in $CuIr_2Te_{3.9}Se_{0.1}$.

Since the lower critical and the upper critical fields ($\mu_0 H_{c1}(0)$ and $\mu_0 H_{c2}(0)$) are essential properties of superconductors, we next estimate the $\mu_0 H_{c1}(0)$ and $\mu_0 H_{c2}(0)$. As represented in figure 4(b), $\mu_0 H_{c1}(T)$ for the optimal compound $CuIr_2Te_{3.9}Se_{0.1}$ has been estimated from the magnetization isotherms in the temperature range 1.8 K–2.8 K (see lower inset of figure 4(b)). The profile of the $M(H)$ curves points that $CuIr_2Te_{3.9}Se_{0.1}$ is a type-II superconductor as evidenced by the linear shielding ('Meissner line') at low fields (see solid straight line in inset). Above ∼300 Oe, the shielding reduces as magnetic flux starts to penetrate the bulk and the system gets in the vortex state. To figure out the $\mu_0 H_{c1}(0)$, we pursued the method which has been used before for different SC as demonstrated in the insets of figure 4(b). The demagnetization effect has been considered to get an accurate value of $\mu_0 H_{c1}(0)$. We can get the demagnetization factor (N) value from the formula $N = 4\pi \chi_V + 1$, where $\chi_V = dM/dH$ is the slope of linear fitting (see the upper inset in figure 4(b)). The estimated value of N is 0.56. As shown in the lower inset of figure 4(b), the fitted purple linear line describes the Meissner shielding effects at low fields based on the formula $M_{Fit} = fH + e$ (Meisner line) in the region of low magnetic fields, where f represents the slope of the linearly fitted $M(H)$ data and e is the intercept. We can subtract Meissner line from the magnetization M for each isotherm ($M - M_{Fit}(H)$) to determine the value of $\mu_0 H_{c1}^*$. As depicted in the top inset in figure 4(b), $\mu_0 H_{c1}^*$ values are determined from 1% M at the field when diverges below the fitted data (M_{Fit}). By considering N, we can obtain $\mu_0 H_{c1}(0)$ from the expression: $\mu_0 H_{c1}(T) = \mu_0 H_{c1}^*(T)/(1 - N)$. We can further calculate the $\mu_0 H_{c1}(T)$ data using the formula: $\mu_0 H_{c1}(T) = \mu_0 H_{c1}(0)\left(1 - \left(\frac{T}{T_c}\right)^2\right)$. The extrapolation of the $\mu_0 H_{c1}(T)$ data down to $T = 0$ K yields the value $\mu_0 H_{c1}(0) = 66$ mT for $CuIr_2Te_{3.9}Se_{0.1}$, which is almost 2.5 times larger than $\mu_0 H_{c1}(0)$ of the parent $CuIr_2Te_4$ (28 mT, see table 2).

The upper critical $\mu_0 H_{c2}(0)$ for the $CuIr_2Te_{3.9}Se_{0.1}$ and $CuIr_2Te_{3.8}Se_{0.2}$ superconducting samples are estimated from low temperature $\rho(T)$ data under different applied fields (between 0 and 500 Oe). The temperature-dependent resistivity is presented in figures 4(c) and (d). The resistivity transition gradually shifts to lower temperatures but seems to be a least susceptible to the applied magnetic field, indicating robust SC. The T_c at each magnetic field is extracted and plotted in the inset of figures 4(c) and (d). The derived $\mu_0 H_{c2}(T)$ diagrams of $CuIr_2Te_{3.9}Se_{0.1}$ and $CuIr_2Te_{3.8}Se_{0.2}$ are plotted in figures 4(c) and (d), respectively. The values of $\mu_0 H_{c2}(0)$ are determined through Ginzberg–Landau (GL) and Werthamer–Helfand–Hohenburg (WHH) theories. We calculated $\mu_0 H_{c2}(0)$ values from the criteria 90%, 50% and 10% of superconducting transition in resistivity data (ρ_N) using the GL equation [53]: $\mu_0 H_{c2}(T) = \mu_0 H_{c2}(0) \times \frac{1 - (T/T_c)^2}{1 + (T/T_c)^2}$. The $\mu_0 H_{c2}(0)$ values from 50% ρ_N criteria are 148 and 127 mT, respectively. On the other hand, the $\mu_0 H_{c2}$ values calculated from the simplified WHH equation for the dirty-limit SC: $\mu_0 H_{c2}(0) = -0.693 \times T_c \backslash (dH_{c2}/dT)|_{T_c}$ [54, 55] where (dH_{c2}/dT_c) denotes the slope
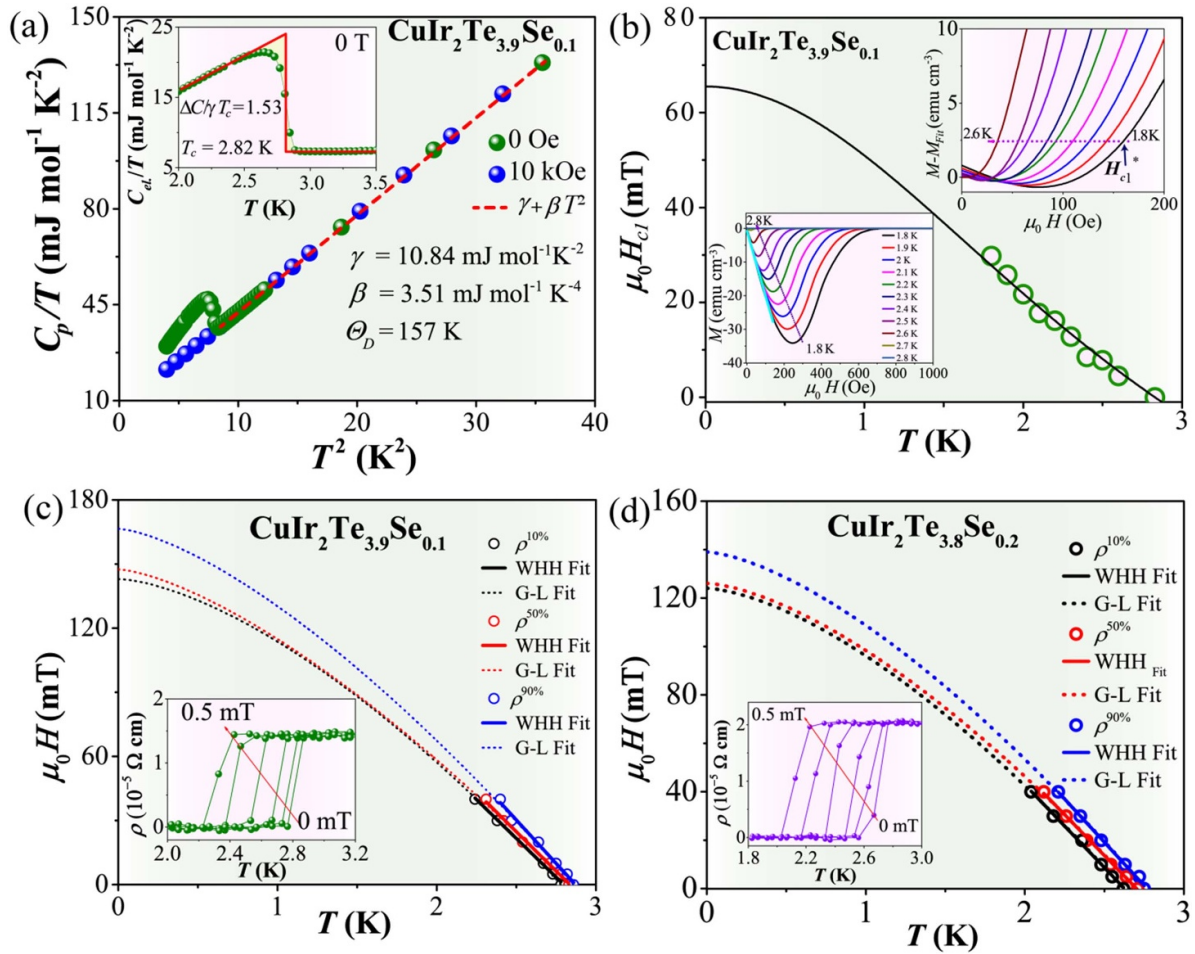
Figure 4. (a) Low-temperature C_p/T at zero (solid green circles) and 10 kOe field (solid blue circles) as a function of T^2, the inset shows C_{el}/T vs T. (b) The lower critical field for CuIr$_2$Te$_{3.9}$Se$_{0.1}$ with the fitting lines using the equation $\mu_0 H_{c1}(T) = \mu_0 H_{c1}(0)\left(1 - \left(\frac{T}{T_c}\right)^2\right)$. The bottom and upper insets illustrate the magnetic susceptibilities $M(H)$ curves and $M - M_{Fit}$ (H) at various temperatures, respectively. ((c) and (d)) The upper critical fields for CuIr$_2$Te$_{3.9}$Se$_{0.1}$ and CuIr$_2$Te$_{3.8}$Se$_{0.2}$. The data are extracted from $\rho(T,H)$ and fitted by GL and WHH models for different criteria. The insets depict the temperature-dependent resistivity under different magnetic field $\rho(T,H)$ curves for CuIr$_2$Te$_{3.9}$Se$_{0.1}$ and CuIr$_2$Te$_{3.8}$Se$_{0.2}$, respectively.

Table 2. Superconducting parameters of different ternary telluride chalcogenides compounds.

Material / Parameter	CuIr$_2$Te$_{3.9}$Se$_{0.1}$ (This work)	CuIr$_2$Te$_{3.8}$Se$_{0.2}$ (This work)	CuIr$_2$Te$_4$ [33]	CuIr$_{1.95}$Ru$_{0.05}$Te$_4$ [58]	CuIr$_2$Te$_{3.9}$I$_{0.1}$ [57]	Cu$_{0.25}$Zn$_{0.25}$IrTe$_2$ [59]
T_c (K)	2.83	2.71	2.5	2.79	2.95	2.82
γ(mJ mol^{-1} K^{-2})	10.84	—	12.05	12.26	12.97	13.37
β (mJ mol^{-1} K^{-4})	3.51	—	1.97	1.87	3.03	1.96
Θ_D (K)	157	—	190	193	165	190.6
$\Delta C/\gamma T_c$	1.51	—	1.5	1.51	1.46	1.45
λ_{ep}	0.65	—	0.63	0.65	0.70	0.66
$N(E_F)$ (states/eV/f.u.)	3.11	—	3.1	3.15	3.24	3.41
$\mu_0 H_{c1}(0)$ (mT)	66	—	28	98	24	62
$\mu_0 H_{c2}(0)$ (mT) ($\rho_{N50\%}$ GL theory)	148	127	145	—	232	198
$\mu_0 H_{c2}(0)$ (mT) ($\rho_{N50\%}$ WHH theory)	144	125	120	247	188	—
$-dH_{c2}/dT_c$ (mT K^{-1})	73.3	66	66	125	—	—
$\mu_0 H^P$ (T)	5.26	5.04	4.65	5.24	5.49	5.26
ξ_{GL} (nm)	47.18	51.34	52.8	36.3	41.9	40.7
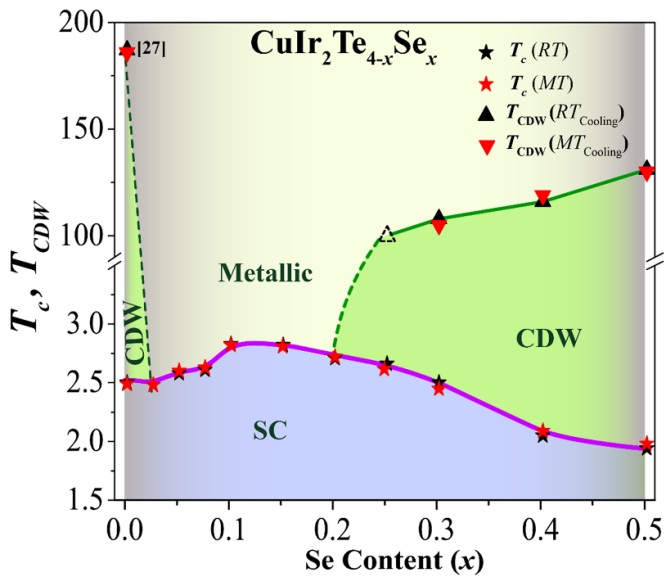
Figure 5. The phase diagram of T_c and T_{CDW} versus Se doping content. The T_c data has been extracted from ρ/ρ_{300K} (T) and $\chi(T)$. T_{CDW} has been extracted from the cooling data of the zero-field ρ/ρ_{300K} (T) and $\chi(T)$ under 10 kOe.

of $\mu_0 H_{c2}(T)$ near T_c (the color solid line). The obtained values of $\mu_0 H_{c2}(0)$ from WHH model for $CuIr_2Te_{4-x}Se_x$ ($x = 0.1$ and 0.2) from the 50% ρ_N criteria are 144 and 125 mT, respectively. The $\mu_0 H_{c2}(0)$ do not surpass the Pauli limiting field for the weak-coupling BCS superconductors $H^P = 1.86 \times T_c$ [56]. Therefore, the values of H^P are estimated to 5.26 and 5.04 T, respectively. The Ginzburg–Landau coherence length ($\xi_{GL}(0)$) is extracted from this equation $H_{c2} = \varphi_0/(2\pi\xi_{GL}^2)$ [56] at the 50% criteria $\mu_0 H_{c2}(0)$, where $\emptyset_0 = 2.07 \times 10^{-3}$ T μm^2 is the flux quantum. $\xi_{GL}(0)$ values for $CuIr_2Te_{3.9}Se_{0.1}$ and $CuIr_2Te_{3.8}Se_{0.2}$ are 47.831 and 51.34 nm, respectively. Table 2 gives a sight about the physical properties of our present studied compounds as compared to other previous reported telluride chalcogenides.

Figure 5 depicts the $T(x)$ phase diagram of T_{CDW} and T_c versus Se content (x) for $CuIr_2Te_{4-x}Se_x$, showing CDW-like order, metallic state and superconducting phase edges. In the beginning, with increasing Se content x, the CDW-like order has vanished around $x = 0.025$. The suppression of CDW-like transition first causes the enhancement of T_c and T_c reach to the highest value of 2.83 K at $x = 0.1$. Nevertheless, with a further increase of Se, the T_c decreases and gives rise to a weak SC dome-like phase diagram. Unexpectedly, the higher Se concentration ($x > 0.2$) induces the reappearance of CDW-like state with a lower transition value than that of the Se-free host material. Such tendency of CDW has been found by iodine doping for Te [57] but not by Zn doping in Cu site or Ru, Al, Ti doping in Ir site [58–60]. Thus, the CDW-like transition in this system seems to be dopant-dependent. Similar behavior has also been reported for Tl-intercalated Nb_3Te_4 single crystals [61], which is ascribed to the disorder in the quasi 1D Nb chains. Besides, M_xTiSe_2 where M is $3d$ transition metal (M = Mn, Cr, Fe) systems also manifested analogous phenomena where CDW was first suppressed

and then re-appeared with higher intercalation concentration, which is due to the deformation degree of Se–Ti–Se sandwiches [62, 63]. The re-occurrence of CDW is reported for 1T-$TaS_{2-x}Se_x$ single crystals as well [64]. One additional case is 2H-$TaSe_{2-x}S_x$ ($0 \leqslant x \leqslant 2$), where a large dome-like superconducting phase diagram is accompanied by the appearance of CDW at two ends [25], where disorder played a significant role in the behavior of CDW and SC. On the other hand, RRR has been widely considered to be an indication of disorder a dirty superconductor [48–50]. It is also well known that RRR ratio is reduced in the dirty-band case [65–68]. However, in our case, RRR ratio increases with increasing doping content in the lower doping region from 0 to 0.1, while decreases as x arises in the higher doping region of 0.1 – 0.5. From figure 5, T_c increases as the CDW transition is suppressed and completely disappears, while the T_c decreases when the CDW transition reemerges and T_{CDW} increased with the doping content. Overall, this system exhibits competing tendencies towards CDW and SC orders. Therefore, we suggest that the initial enhancement of the T_c and disappearance of the CDW is due to the increase of DOS at FS and the reemergence of CDW in over Se-doped region might result from the disorder scattering of Se-impurities and the decrease of DOS at FS because some portions of FS are removed by CDW gaping and consequently degrading superconducting T_c [68]. Yet, further theoretical and/or experimental studies need to prove it.

4. Conclusion

In summary, our results highlighted the role of Se doping in SC and CDW-like states on $CuIr_2Te_{4-x}Se_x$. We have successfully synthesized a series of $CuIr_2Te_{4-x}Se_x$ ($0 \leqslant x \leqslant 0.5$) polycrystalline compounds. PXRD results from different temperatures demonstrate that the trigonal phase is stable at 20, 100 K and 300 K, indicating there is no structural phase transition at low temperature. By the means of the electrical resistivity, magnetic susceptibility and specific heat measurements of $CuIr_2Te_{4-x}Se_x$ ($0 \leqslant x \leqslant 0.5$) compounds, it can be found that when Se substitution concentrations in the range of $x \leqslant 0.2$, the Se substitution leads to the disappearance of the CDW-like state. Besides, a slight increase of T_c can be seen with the highest T_c of about 2.83 K for the optimal doping $x = 0.10$. However, further augmentation of the dopant content ($x \geqslant 0.25$) caused the reappearance of noticeable anomalies in both resistivity and magnetization, indicating the CDW-like transition retakes place, which is highly related to the disorder effects created by selenium doping. Nevertheless, these findings call for further studies to determine the possible explanations behind this kind of behavior.

Data availability statement

The data that support the findings of this study are openly available at the following URL/DOI: http://dx.doi.org/10.2139/ssrn.3761880.

Acknowledgments

ORCID iDs

Jinguang Cheng ⓘ https://orcid.org/0000-0002-4969-1960
Yingying Peng ⓘ https://orcid.org/0000-0002-2657-3590
Huixia Luo ⓘ https://orcid.org/0000-0003-2703-5660

References

[1] Hsu Y T, Vaezi A, Fischer M H and Kim E A 2017 Topological superconductivity in monolayer transition metal dichalcogenides *Nat. Commun.* **8** 14985

[2] Kononov A, Abulizi G, Qu K, Yan J, Mandrus D, Watanabe K, Taniguchi T and Schönenberger C 2020 One-dimensional edge transport in few-layer WTe$_2$ *Nano Lett.* **20** 4228–33

[3] Wang L, Rosdahl T O and Sticlet D 2018 Platform for nodal topological superconductors in monolayer molybdenum dichalcogenides *Phys. Rev.* B **98** 205411

[4] Lin D *et al* 2020 Patterns and driving forces of dimensionality-dependent charge density waves in 2H-type transition metal dichalcogenides *Nat. Commun.* **11** 2406

[5] Straub T, Finteis T, Claessen R, Steiner P, Hüfner S, Blaha P, Oglesby C S and Bucher E 1999 Charge-density wave mechanism in 2H-NbSe$_2$: photoemission results *Phys. Rev. Lett.* **82** 4504–7

[6] Lian C-S, Si C and Duan W 2018 Unveiling charge-density wave, superconductivity, and their competitive nature in two-dimensional NbSe$_2$ *Nano Lett.* **18** 2924–9

[7] Hsu Y-T, Vaezi A, Fischer M H and Kim E-A 2017 Topological superconductivity in monolayer transition metal dichalcogenides *Nat. Commun.* **8** 14985

[8] Luo H, Klimczuk T, Müchler L, Schoop L, Hirai D, Fuccillo M K, Felser C and Cava R J 2013 Superconductivity in the Cu(Ir$_{1-x}$Pt$_x$)$_2$Se$_4$ spinel *Phys. Rev.* B **87** 214510

[9] Leng H, Paulsen C, Huang Y K and de Visser A 2017 Type-I superconductivity in the Dirac semimetal PdTe$_2$ *Phys. Rev.* B **96** 220506

[10] Teknowijoyo S, Jo N H, Scheurer M S, Tanatar M A, Cho K, Bud'ko S L, Orth P P, Canfield P C and Prozorov R 2018 Nodeless superconductivity in the type-II Dirac semimetal PdTe$_2$: London penetration depth and pairing-symmetry analysis *Phys. Rev.* B **98** 024508

[11] Kim H-S, Haule K and Vanderbilt D 2019 Mott metal-insulator transitions in pressurized layered trichalcogenides *Phys. Rev. Lett.* **123** 236401

[12] Alekseev P S, Dmitriev A P, Gornyi I V and Kachorovskii V Y 2013 Strong magnetoresistance of disordered graphene *Phys. Rev.* B **87** 165432

[13] Dayen J-F, Ray S J, Karis O, Vera-Marun I J and Kamalakar M V 2020 Two-dimensional van der Waals spinterfaces and magnetic-interfaces *Appl. Phys. Rev.* **7** 011303

[14] Luo H X *et al* 2015 Cr-doped TiSe$_2$—a layered dichalcogenide spin glass *Chem. Mater.* **27** 6810–7

[15] Suderow H, Tissen V G, Brison J P, Martínez J L and Vieira S 2005 Pressure induced effects on the Fermi surface of superconducting 2H-NbSe$_2$ *Phys. Rev. Lett.* **95** 117006

[16] Denholme S J, Yukawa A, Tsumura K, Nagao M, Tamura R, Watauchi S, Tanaka I, Takayanagi H and Miyakawa N 2017 Coexistence of superconductivity and charge-density wave in the quasi-one-dimensional material HfTe$_3$ *Sci. Rep.* **7** 45217

[17] Morosan E, Zandbergen H W, Dennis B S, Bos J W G, Onose Y, Klimczuk T, Ramirez A P, Ong N P and Cava R J 2006 Superconductivity in Cu$_x$TiSe$_2$ *Nat. Phys.* **2** 544–50

[18] Kudo K, Kobayashi M, Pyon S and Nohara M 2013 suppression of structural phase transition in IrTe$_2$ by isovalent Rh doping *J. Phys. Soc. Japan* **82** 085001

[19] Yang J J, Choi Y J, Oh Y S, Hogan A, Horibe Y, Kim K, Min B I and Cheong S W 2012 Charge-orbital density wave and superconductivity in the strong spin-orbit coupled IrTe$_2$: Pd *Phys. Rev. Lett.* **108** 116402

[20] Jin K and Liu K 2015 What drives superconductivity in Pt-doped IrTe$_2$? *Sci. Bull.* **60** 822

[21] Kudo K, Ishii H, Takasuga M, Iba K, Nakano S, Kim J, Fujiwara A and Nohara M 2013 Superconductivity induced by breaking Te$_2$ dimers of AuTe$_2$ *J. Phys. Soc. Japan* **82** 063704

[22] Kamitani M, Bahramy M S, Arita R, Seki S, Arima T, Tokura Y and Ishiwata S 2013 Superconductivity in Cu$_x$IrTe$_2$ driven by interlayer hybridization *Phys. Rev.* B **87** 180501

[23] Xi X, Berger H, Forró L, Shan J and Mak K F 2016 Gate tuning of electronic phase transitions in two-dimensional NbSe$_2$ *Phys. Rev. Lett.* **117** 106801

[24] Liu Y, Ang R, Lu W J, Song W H, Li L J and Sun Y P 2013 Superconductivity induced by Se-doping in layered charge-density-wave system 1T-TaS$_{2-x}$Se$_x$ *Appl. Phys. Lett.* **102** 192602

[25] Li L *et al* 2017 Superconducting order from disorder in 2H-TaSe$_{2-x}$S$_x$ *npj Quantum Mater.* **2** 11

[26] Luo H X, Xie W W, Tao J, Inoue H, Gyenis A, Krizan J W, Yazdani A, Zhu Y and Cava R J 2015 Polytypism, polymorphism, and superconductivity in TaSe$_{2-x}$Te$_x$ *Proc. Natl Acad. Sci.* **112** E1174

[27] Benedičič I *et al* 2020 Superconductivity emerging upon Se doping of the quantum spin liquid 1T-TaS$_2$ *Phys. Rev.* B **102** 054401

[28] Liu W H, Osanloo M R, Wang X Q, Li S, Dhale N, Wu H L, van de Put M L, Tiwari S, Vandenberghe V G and Lv B 2021 New Verbeekite-type polymorphic phase and rich phase diagram in the PdSe$_{2-x}$Te$_x$ system *Phys. Rev.* B **104** 024507

[29] Liu W H, Li S, Wu H L, Dhale N, Koirala P and Lv B 2021 Enhanced superconductivity in the Se-substituted 1T-PdTe$_2$ *Phys. Rev. Mater.* **5** 014802

[30] Hoesch M, Gannon L, Shimada K, Parrett B J, Watson M D, Kim T K, Zhu X D and Petrovic C 2019 Disorder quenching of the charge density wave in ZrTe$_3$ *Phys. Rev. Lett.* **122** 017601

[31] Zhang P *et al* 2015 Superconductivity enhanced by Se doping in Eu$_3$Bi$_2$(S,Se)$_4$F$_4$ *Europhys. Lett.* **111** 27002

[32] Niu C Q, Yang J H, Li Y K, Chen B, Zhou N, Chen J, Yang X X, Cao C, Dai J and Xu X 2013 Effect of selenium

doping on the superconductivity of Nb$_2$Pd(S$_{1-x}$Se$_x$)$_5$ *Phys. Rev.* B **88** 104507

[33] Yan D *et al* 2019 CuIr$_2$Te$_4$: a quasi-two-dimensional ternary telluride chalcogenide superconductor (arXiv:1908.05438)

[34] Erkişi A 2019 Magnetic orders and electronic behaviours of new chalcogenides Cu$_3$MnCh$_4$ (Ch = S, Se and Te): an *ab initio* study *Phil. Mag.* **99** 1941–55

[35] Moris S, Valencia-Gálvez P, Mejía-López J, Peña O, Barahona P and Galdámez A 2019 CuCr$_{2-x}$Sn$_x$S$_{4-y}$Se$_y$ Spinels: crystal structure, density functional theory calculations, and magnetic behavior *Inorg. Chem.* **58** 13945–52

[36] Ramasamy K, Sims H, Gupta R K, Kumar D, Butler W H and Gupta A 2013 Co$_x$Cu$_{1-x}$Cr$_2$S$_4$ nanocrystals: synthesis, magnetism, and band structure calculations *Chem. Mater.* **25** 4003–9

[37] Endoh R, Matsumoto N, Awaka J, Ebisu S and Nagata S 2002 Metal-insulator transition in the spinel-type Cu(Ir$_{1-x}$Cr$_x$)$_2$S$_4$ system *J. Phys. Chem. Solids* **63** 669–74

[38] Matsumoto N, Yamauchi Y, Awaka J, Kamei Y, Takano H and Nagata S 2001 Metal–insulator transition in the spinel-type Cu(Ir$_{1-x}$Pt$_x$)$_2$S$_4$ system *Int. J. Inorg. Mater.* **3** 791–5

[39] Nagata S, Hagino T, Seki Y and Bitoh T 1994 Metal-insulator transition in thiospinel CuIr$_2$S$_4$ *Physica* B **194–6** 1077–8

[40] Miyatani K, Tanaka T, Sakita S, Ishikawa M and Snirakawa N 1993 Magnetism and superconductivity in copper spinels *Japan. J. Appl. Phys.* **32** 448

[41] Cao G, Kitazawa H, Suzuki H, Furubayashi T, Hirata K and Matsumoto T 2000 Superconductivity in Zn-doped CuIr$_2$S$_4$ *Physica* C **341–8** 735–6

[42] Hagino T, Seki Y, Wada N, Tsuji S, Shirane T, Kumagai K I and Nagata S 1995 Superconductivity in spinel-type compounds CuRh$_2$S$_4$ and CuRh$_2$Se$_4$ *Phys. Rev.* B **51** 12673–84

[43] Furubayashi T, Kosaka T, Tang J, Matsumoto T, Kato Y and Nagata S 1997 Pressure induced metal-insulator transition of selenospinel CuIr$_2$Se$_4$ *J. Phys. Soc. Japan* **66** 1563–4

[44] Irizawa A, Kobayashi M, Satoh K, Nanba T, Chen L, Matsumoto T, Matsunami M, Ito M, Suzuki T and Nagata S 2007 Study on cross-over change from metal to insulator in the electronic states of copper-spinel compounds under high pressure *J. Phys. Soc. Japan* **76** 13–14

[45] Burkov A T, Nakama T, Hedo M, Shintani K, Yagasaki K, Matsumoto N and Nagata S 2000 Anomalous resistivity and thermopower of the spinel-type compounds CuIr$_2$S$_4$ and CuIr$_2$Se$_4$ *Phys. Rev.* B **61** 10049–56

[46] Denton A R and Ashcroft N W 1991 Vegard's law *Phys. Rev.* A **43** 3161–4

[47] Bagnall K W 1973 *In the Chemistry of Sulphur, Selenium, Tellurium and Polonium* ed M Schmidt, W Siebert and K W Bagnall (Pergamon: Elsevier) pp 935–1008

[48] Wang X-L, Dou S X, Hossain M S A, Cheng Z X, Liao X Z, Ghorbani S R, Yao Q W, Kim J H and Silver T 2010 Enhancement of the in-field J_c of MgB$_2$ via SiCl$_4$ doping *Phys. Rev.* B **81** 224514

[49] de Silva K S B, Xu X, Wang X L, Wexler D, Attard D, Xiang F and Dou S X 2012 A significant improvement in the superconducting properties of MgB$_2$ by co-doping with graphene and nano-SiC *Scr. Mater.* **67** 802–5

[50] Wang H T, Li L J, Ye D S, Cheng X H and Xu Z A 2007 Effect of Te doping on superconductivity and charge-density wave in dichalcogenides 2H-NbSe$_{2-x}$Te$_x$ ($x = 0, 0.1, 0.2$) *Chin. Phys.* **16** 2471

[51] Cao H, Chakoumakos B C, Chen X, Yan J, McGuire M A, Yang H, Custelcean R, Zhou H, Singh D J and Mandrus D 2013 Origin of the phase transition in IrTe$_2$: structural modulation and local bonding instability *Phys. Rev.* B **88** 115122

[52] McMillan W L 1968 Transition temperature of strong-coupled superconductors *Phys. Rev.* **167** 331–44

[53] Ginzburg V L 1955 On the theory of superconductivity *Il Nuovo Cimento* **2** 1234–50

[54] Kohn W 1967 Excitonic phases *Phys. Rev. Lett.* **19** 439–42

[55] Werthamer N R and McMillan W L 1967 Temperature and purity dependence of the superconducting critical field Hc$_2$ IV. Strong-coupling effects *Phys. Rev.* **158** 415–7

[56] Clogston A M 1962 Upper limit for the critical field in hard superconductors *Phys. Rev. Lett.* **9** 266–7

[57] Boubeche M *et al* 2021 Superconductivity and charge density wave in iodine-doped CuIr$_2$Te$_4$ *Chin. Phys. Lett.* **38** 037401

[58] Yan D *et al* 2019 Superconductivity in Ru-doped CuIr$_2$Te$_4$ telluride chalcogenide *Phys. Rev.* B **100** 174504

[59] Yan D, Zeng Y, Lin Y, Zeng L, Yin J, Boubeche M, Wang M, Wang Y, Yao D-X and Luo H 2021 Robust superconductivity in (Zn$_x$Cu$_{1-x}$)$_{0.5}$IrTe$_2$ *J. Phys. Chem.* C **125** 5732–8

[60] Yan D *et al* 2020 Charge density wave and superconductivity in the family of telluride chalcogenides Zn$_{1-x}$Cu$_x$Ir$_{2-y}$N(N = Al, Ti, Rh)$_y$Te$_4$ (arXiv:2003.11463)

[61] Scholz G A 1997 Charge-density-wave behaviour in intercalated single crystal Nb$_3$Te$_4$ *Solid State Ion.* **100** 135–41

[62] Baranov N V, Maksimov V I, Mesot J, Pleschov V G, Podlesnyak A, Pomjakushin V and Selezneva N V 2006 Possible reappearance of the charge density wave transition in M$_x$TiSe$_2$ compounds intercalated with 3d metals *J. Phys.: Condens. Matter* **19** 016005

[63] Selezneva N V, Sherokalova E M, Pleshchev V G, Kazantsev V A and Baranov N V 2016 Suppression and inducement of the charge-density-wave state in Cr$_x$TiSe$_2$ *J. Phys.: Condens. Matter* **28** 315401

[64] Liu Y *et al* 2016 Nature of charge-density-wave and superconductivity in 1T-TaSe$_{2-x}$Te$_x$ *Phys. Rev.* B **94** 041531

[65] Anderson P W 1959 *Phys. Rev. Lett.* **3** 325

[66] Zhu X, Lv B, Wei F, Xue Y, Lorenz B, Deng L, Sun Y and Chu C-W 2013 Disorder-induced bulk superconductivity in ZrTe$_3$ single crystals via growth control *Phys. Rev.* B **87** 024508

[67] Barnett R L, Polkovnikov A, Demler E, Yin W G and Ku W 2006 Coexistence of gapless excitations and commensurate charge-density wave in the 2H transition metal dichalcogenides *Phys. Rev. Lett.* **96** 026406

[68] Harper J M, Geballem T E and Disalvo F J 1977 Thermal properties of layered transition-metal dichalcogenides at charge-density-wave transitions *Phys. Rev.* B **15** 2943–51